Macromolecular imprinting of peptide nucleic acid resulting in an electropolymerized sequence-controlled CG-rich artificial oligomer analog for improved oligonucleotide determination

Journal:	*ACS Applied Materials & Interfaces*
Manuscript ID	Draft
Manuscript Type:	Letter
Date Submitted by the Author:	n/a
Complete List of Authors:	Bartold, Katarzyna; Institute of Physical Chemistry of the Polish Academy of Sciences Pietrzyk-Le, Agnieszka; Institute of Physical Chemistry of the Polish Academy of Sciences, Department of Physical Chemistry of Supramolecular Complexes Golebiewska, Karolina; Institute of Physical Chemistry, Polish Academy of Sciences Lisowski, Wojciech; Institute of Physical Chemistry, Polish Academy of Sciences Cauteruccio, Silvia; Università degli Studi di Milano, Chemistry Licandro, Emanuela; Univeristy of Milan, Department of Organic and Industrial Chemistry D'Souza, Francis; University of North Texas,, Department of Chemistry Kutner, Wlodzimierz; Institute of Physical Chemistry of the Polish Academy of Sciences, Department of Physical Chemistry of Supramolecular Complexes

Macromolecular imprinting of peptide nucleic acid resulting in an electropolymerized sequence-controlled CG-rich artificial oligomer analog for improved oligonucleotide determination

Katarzyna Bartold,[a] *Agnieszka Pietrzyk-Le,*[a,*] *Karolina Golebiewska,*[a] *Wojciech Lisowski,*[a] *Silvia Cauteruccio,*[b] *Emanuela Licandro,*[b] *Francis D'Souza,*[c] *and Wlodzimierz Kutner*[a, d]

[a] Institute of Physical Chemistry, Polish Academy of Sciences, Kasprzaka 44/52, 01-224 Warsaw, Poland

[b] Department of Chemistry, University of Milan, Via Golgi, 19 I-20133 Milan, Italy

[c] Department of Chemistry, University of North Texas, Denton, 1155, Union Circle, #305070 TX 76203-5017, USA

[d] Faculty of Mathematics and Natural Sciences, School of Sciences, Cardinal Stefan Wyszynski University in Warsaw, Wóycickiego 1/3, 01-938 Warsaw, Poland

KEYWORDS: DNA sensor, CG-rich DNA analog, peptide nucleic acid, PNA, macromolecularly imprinted polymer, hybridization, ITC, conformational change

ABSTRACT

Using a 'macromolecular imprinting in polymer strategy' and a sequence-programmable peptide nucleic acid (PNA) template, we electrosynthesized and electrode immobilized a sequence-defined *octakis*(2,2'-bithien-5-yl) DNA hybridizing probe. Fabrication of this octamer probe in molecular cavities of the molecularly imprinted polymer (MIP) tuned this probe density, thus revealing appreciable and reproducible hybridization efficiency. With highly sensitive and simple to operate EIS and SPR transductions under stagnant-solution and FIA conditions, respectively, we determined genetically relevant GCGGCGGC (G-guanine, C-cytosine) oligonucleotide with the 200 pM EIS limit of detection. The chemosensor was selective to mismatched oligonucleotides and discriminative to Dulbecco Modified Eagle Medium sample interferences.

Several strategies have already been developed for qualitative and quantitative DNA determination.[1-2] They include optical, mass-sensitive, and electrochemical methods.[3-5] Particularly, the latter has a great potential in the DNA sensor technology development because of low cost, simplicity, and ease of miniaturization.[1, 6-7] However, more research efforts should be devoted to improve the proposed DNA sensing procedures for the point-of-care applications. Toward this goal, highly sensitive, selective, and rapid DNA determination, with simplified protocols and with as limited as possible sample preparation, is of paramount importance.

Many electrochemical systems for DNA sensing use biological recognition units capable of hybridizing a single-stranded DNA (ssDNA) analyte.[8-11] To minimize drawbacks of the challenging control of the density and orientation of natural probes and time-consuming optimization of the solution conditions for analyte-probe hybridization,[12] several nucleic acid analogs were designed and synthesized,[13-16] and then used as the probes.[17-19]

Among them, peptide nucleic acids (PNAs) were selected, because of their sequence-selectivity and high affinity to complementary DNA and RNA single strands. However, they often need backbone and nucleobase modifications in order to pre-organize[20] their conformation, and then increase stability and sequence selectivity in duplex formation. Moreover, PNA modification results from the way of its further immobilization on the transducer surface. This step is crucial because it affects the sensitivity and selectivity of the resulting chemosensor.[21-22]

Moreover, time-consuming procedures of preparation of recognition films may hinder further development of DNA determination methods. For instance, a transducer surface was modified with PNA by exposing a gold substrate to a thiolated-PNA solution for ~10 h.[23] A similarly long procedure was necessary for preparation of the thiolated-PNA probe modified electrodes by self-assembled monolayer formation.[24] Moreover, the assay

sensitivity with these immobilization procedures was expected to be critically dependent upon both the probe surface density and the ionic strength of the buffer solution used. In an example of the PNA covalently attached to a quinone-based electroactive polymer via the amide bond, an electrochemical response was straightforward.[25] However, preparation of a PNA modified electrode was highly demanding.

Another parameter governing the use of the PNA is the distance between the modified PNA and the electrode surface. Apparently, the length and the terminating head group of blocking thiol molecules influenced the sensitivity and selectivity of label-free capacitive DNA detection using an immobilized pyrrolidinyl PNA probe.[26]

By engaging the molecular imprinting in polymer strategy, we have recently developed a fast, cost-effective, and simple procedure of one-step synthesis of a new electropolymerized DNA analog probe.[17] Moreover, the hybridizing probe was simultaneously immobilized on the transducer surface in this procedure. Using this macromolecular imprinting, we improved the orientation of the probes, thus tuning their density, which in turn influenced the hybridization yield. Furthermore, we enhanced utility of our strategy toward development of point-of-care devices. For that, we coupled a readily prepared recognizing probe with highly sensitive electrochemical impedance spectroscopy, EIS, signal transducer offering a great opportunity of miniaturization. Therefore, straightforward, rapid, and label-free DNA quantification was possible.

The present research aims at identification of genetically relevant GC-rich oligonucleotides, e.g., cancer biomarkers encountered in the bloodstream as a cell-free DNA. Furthermore, it is oriented for detection of some pathogens, e.g., *Pseudomonas aeruginosa*, which have high specific GC content in their genome. For that, we used a new cytosine-guanine (CG) rich *octakis*(2,2'-bithien-5-yl)methane DNA analog probe of the defined

structure capable of hybridizing a complementary GC-rich (GCGGCGGC) octanucleotide analyte.

For the synthesis of this new probe, we used PNA **1** (Scheme 1) as the template, around which 2-(cytosin-1-yl)ethyl 4-*bis*(2,2'-bithien-5-yl)methylbenzoate **2** (Scheme 1) and 4-*bis*(2,2'-bithien-5-yl)methylphenyl-2-guanine ethyl ether **3** (Scheme 1) functional monomers arranged by assuming positions governed by the complementary nucleobase pairing rule.

Binding nature of the designed and synthesized functional monomers with PNA was confirmed by isothermal titration calorimetry (ITC). All complex stability constants determined by ITC titrations (Figure 1) of PNA with **3** or **2** indicated a very strong binding interaction (Table 1). The determined ITC thermodynamic parameters revealed that functional monomers bearing complementary nucleobases presumably bound to PNA via Watson-Crick nucleobase pairing. We demonstrated that nucleobase moieties of functional monomers were involved in recognition of binding sites of PNA (Table 1). The GCGGCGGC PNA oligonucleotide, composed of three cytosine binding sites, formed a stable complex ($K_s = 1.5\times10^5$ M^{-1}) with three molecules of guanine functional monomer **3** (Table 1). From the ITC raw heat rate change with time during titration of **1** with **3** (Figure 1a), the binding isotherm (Figure 1b) was derived (for details, see Supporting Information).

Moreover, the ITC result confirmed favorable conformational changes of the G-rich PNA during complex formation, which prompted complete pairing with cytosine functional monomer **2** in solution. That is, there were two distinct steps in the isotherm (Figure 1d) derived from the ITC raw heat rate change accompanying titration of **1** with **2** (Figure 1c). These steps indicate consecutive attachment of three, and then two molecules of **2** to the PNA molecule (for details, see Supporting Information). Because of these enthalpy-

dominated effects, all five available guanine recognizing sites of PNA were bound by the cytosine moieties of **2**, thus successfully forming the pre-polymerization complex.

Apparently, the designed and synthesized 2,2'-bithien-5-yl functional monomers bind the PNA template according to the complementary nucleobase Watson-Crick pairing rule, however, through different equilibrium states. Astonishingly, **2** can accelerate activation of the PNA by inducing its conformational changes. Structure of the PNA bound by **2** was slowly rearranged, thus reaching equilibrium between two dominating PNA conformations. This rearrangement necessary to bind all nucleobase sites of the PNA by nucleobase substituents of the functional monomers as well as to form a pre-polymerization complex of high stability (K_s=10^7 M^{-1}). Presumably, this extraordinary mechanism of PNA complex formation by functional monomers promote this complex oligomerization to more stable 2,2'-bithien-5-yl DNA analog in the MIP.

Guided by to the ITC determined stoichiometry, we prepared a mixed solvent solution for electropolymerization of 0.02 mM PNA, 0.1 mM **2**, 0.06 mM **3**, 0.1 mM **4**, and 0.1 M (TBA)ClO_4 at the acetonitrile-to-water volume ratio of 9:1. By taking advantage of electroactivity of *bis*(2,2-bithen-5-yl) moieties of the functional monomers, we readily transferred the pre-polymerization complexes from solution into the MIP film within a few minutes. These films were simultaneously prepared and deposited on the electrode surface by potentiodynamic electropolymerization. For the PNA-imprinted MIP film deposition on the Pt disk, two anodic peaks appeared during the initial positive potential scan (solid curve in Figure 2a). The first peak, originally present at ~1.02 V, completely vanished in two last cycles. The second peak, initially present at ~1.13 V, shifted positively in subsequent cycles. Apparently, the initially deposited MIP layer played a role of the resistive barrier for subsequent MIP layers, thus hindering further electro-oxidation of the monomers present in the solution.

Noticeably, none of these anodic peaks corresponded to PNA template electro-oxidation. Although the PNA template was rich in G, i.e., the most redox-active nucleobase,[27] the guanine moiety stayed in its intact form during the potential cycling (dashed curve in Figure 2a). Apparently, the herein recorded anodic peaks originated from electro-oxidation of thiophene moieties of functional monomers **2** and **3**, and the cross-linking monomer **4**. This is because these peaks were also present in multi-cycle potentiodynamic curves of all cycles corresponding to electropolymerization of **2** and **3** in the PNA absence (Figure 2b), which led to deposition of a control non-imprinted (NIP) film.

After the electropolymerization, the PNA template was extracted from the resulting MIP film (see Supporting Information) in order to vacate imprinted cavities and make them available for the GCGGCGGC DNA analyte molecules. This extraction was confirmed by the XPS (Table S1), DPV (Figure S1), and EIS (Figure S2 in Supporting Information) measurements.

The PNA-templated, and then extracted MIP films as well as the NIP film were imaged with AFM in order to unravel their morphology and determine their thickness (Table S2 in Supporting Information).

The PNA-extracted MIP film was treated as a porous membrane, which contained a matrix formed by the conducting polymer and pores filled with the electrolyte. Two partially superimposed semicircles in the complex plane plot (Figure S2 in Supporting Information) represented a porous structure of the MIP film and redox reaction of the marker, similarly as postulated previously.[28-29] For experimental data interpretation, see Supporting Information.

After extraction of the PNA template from the MIP, empty molecularly imprinted cavities with the C and G sites of the defined sequence were generated, thus resembling an ssDNA. These cavities were capable of binding the GCGGCGGC DNA analyte with high

affinity and selectivity, as confirmed by the EIS (Figure 3) and SPR (Figure S3 in Supporting Information) determinations.

Figure 3a presents Nyquist plots for the MIP chemosensor immersed for 5 min in GCGGCGGC DNA analyte solutions of different concentrations. The experimental data were fitted with electric parameters of the equivalent circuit (Figure S2 in Supporting Information) and charge transfer resistance, R_{ct}, values were determined. The R_{ct} was dependent upon the extent of the analyte occupation of the MIP cavities, as demonstrated by the R_{ct} dependence on the GCGGCGGC DNA analyte concentration in solution (inset in Figure 3a). The chemosensor response was proportional to the analyte concentration in the 3.0-to-80.0 nM range (line *1* in inset to Figure 3a). The linear regression equation and the correlation coefficient of the calibration plot (line *1* in inset to Figure 3a) was $(R_{ct,f} - R_{ct,i})$ [Ω] = 780(±9.0) [Ω] + 55.53(±0.28) [Ω nM^{-1}] $c_{analyte}$ [nM] and 0.99, respectively, where $R_{ct,i}$ and $R_{ct,f}$ is the charge-transfer resistance of the MIP film before and after oligonucleotide analyte injection, respectively. The sensitivity and LOD at S/N=3 was 53(±0.002) Ω nM^{-1} and 200 pM, respectively. Apparently, the MIP chemosensor was ~3.0 times more selective to the GCGGCGGC DNA analyte than to the two-nucleobase mismatches, GCG**AT**GGC DNA and GC**T**GC**T**GC PNA (lines *2'* and *3'* in Figure 3b), and ~3.8 times more sensitive than to its three-nucleobase mismatch, GCG**ATC**GC DNA (line *4'* in Figure 3b). Moreover, the GCGGCGGC DNA analyte was determined using the NIP film (line *2* in inset to Figure 3a). Sensitivity of this film to the analyte, 15(±0.70) Ω nM^{-1}, was nearly four times lower than that of the MIP film, thus indicating that the apparent imprinting factor was, IF ≈ 4.0.

Further, the GCGGCGGC DNA analyte binding by the PNA-extracted MIP film was monitored by SPR spectroscopy under FIA conditions (Figure S3a in Supporting Information). From the ratio of slopes of the SPR calibration plots for the MIP (line *1* in

Figure S3b in Supporting Information) and the NIP film (line *4* in Figure S3b in Supporting Information), the imprinting factor was calculated. It was, IF=11, thus largely exceeding the IF determined for the EIS chemosensor, above. This is presumably because SPR signals are not exclusively mass change governed but also they can conformationally be induced.[30] We assumed that the SPR recorded signals corresponded to conformational changes of the resulted 2,2'-bithien-5-yl DNA analog and the DNA analyte upon hybridization. From the SPR and ITC studies it follows, that the MIP cavities enhanced conformational GCGGCGGC DNA changes required for its hybridization with complementary *octakis*(2,2'-bithien-5-yl) DNA analog. The MIP acted as a receptor of the DNA analyte catalyzing its conformational restructuring before hybridization with the MIP cavity. Moreover, this MIP exhibited enzyme-like behavior. However, it was simultaneously invulnerable to the surrounding conditions, such as pH, temperature, and mass-transfer of substrates. From the ITC measurements it follows that the conformational change in the GC-rich DNA leads to two plausible MIP-bound DNA conformers that are in equilibrium with the MIP cavity. Furthermore, a slow structural conformation change in the DNA analyte occurring upon binding to the MIP cavity may be required for biological activity. Subsequently, this restructuring allows protein anchoring in the MIP film.

The real-time SPR measurement of the analyte-analog hybridization revealed a relatively fast kinetics (k_a=10^4 $M^{-1}s^{-1}$, k_d=10^{-3} s^{-1}) of analyte binding to the MIP cavity and a high stability constant (K_s≈10^7 M^{-1}) of the (analyte)-[*octakis*(2,2'-bithien-5-yl) DNA analog] complex (Table 1 and Figure S4 in Supporting Information). Moreover, the SPR measurement provided data for calculation of hybridization efficiency, which was as high as ~90%. In comparison to octamers of nucleic acid analogs, the MIP cavity bound the complementary DNA analyte much faster and stronger and, importantly, at room temperature.

Vulnerability of DNA determination to the matrix effect of complex matrices is an important criterion of usefulness of a DNA determination procedure. Therefore, we studied the performance of our MIP chemosensor in a complex Dulbecco Modified Eagle Medium (DMEM) resembling low-molecular-weight blood plasma. Toward that, first, the EIS measurements were performed for the analyte of known concentration added to DMEM. Then, this EIS signal was compared to that for the analyte of the same concentration dissolved in PBS (pH=7.4). From the ratio of these two EIS signals, the matrix effect was determined (Table 2). Advantageously, the MIP chemosensor appeared to be independent of the matrix effect.

To conclude, we developed a simple, fast, and catalyst-free procedure of synthesis of a stable *octakis*bithiophene CG-rich oligonucleotide analog for oligonucleotide chemosensing via molecular imprinting. For pre-polymerization complex formation, we chose PNA as the template because it was able to change favorably its conformation under complexation conditions with specially designed and synthesized *bis*(2,2'-bithienyl-5-yl)methane functional monomers, bearing either G or C moiety, for mimicking natural G and C nucleobase pairing. The combination of electrochemical and mass transduction techniques with the synthesis of a new DNA analog allowed fabricating the chemosensor for determination of genetically relevant oligonucleotide. In GC-rich regions, with the hydrogen bond strength higher than that of the AT-rich region, a point mutation might only cause a very slight change in the thermodynamics and local conformation of the duplex, making it very difficult to detect. Our ITC measurements confirmed higher stability of the G-C pairs of the functional monomers with PNA than that of the A-T pairs.[17] Nevertheless, we still successfully and independently from matrix effects discriminated GC-rich analyte from two- and three-nucleobase mismatches with the appreciably low LOD.

ASSOCIATED CONTENT

Supporting Information

The synthesis of **3**, materials and chemicals as well as instrumentation and procedures, deposition of the MIP and NIP films, and their preparation for analyte determination, and then template extraction from the MIP, experimental data of ITC, AFM, XPS, DPV, EIS measurements, the equivalent electric circuit, and SPR kinetics are described in Supporting Information.

AUTHOR INFORMATION

Corresponding Author

*E-mail addresses: apietrzyk@ichf.edu.pl

Author contributions

The manuscript was prepared through contributions of all authors. All authors have given approval to the final version of the manuscript.

Acknowledgments

We thank Prof. Tiziana Benincori (University of Insubria, Como, Italy) for synthesizing the cross-linking monomer **4** and Dr. Marta Sosnowska (IPC PAS, Warsaw, Poland) for synthesis of the functional monomers **2** and **3**. Moreover, we are thankful to Dr. T. Kamiński and Dr. Eng. M. Dabrowski (IPC PAS, Warsaw, Poland) for insightful discussions on nucleic acids. The Parent-Bridge Programme (Grant No. POMOST/2012-6/10 to A.P.-L.) of the Foundation for Polish Science, cofinanced by the European Union Regional Development Fund, financially supported the present research.

References

1. Li, D.; Song, S.; Fan, C. H., Target-Responsive Structural Switching for Nucleic Acid-Based Sensors. *Acc. Chem. Res.* **2010,** *43*, 631-641.
2. Du, Y.; Dong, S., Nucleic Acid Biosensors: Recent Advances and Perspectives. *Anal. Chem.* **2017,** *89*, 189-215.
3. Sassolas, A.; Leca-Bouvier, B. D.; Blum, L. J., DNA Biosensors and Microarrays. *Chem. Rev.* **2008,** *108*, 109-139.
4. Teles, F. R. R.; Fonseca, L. P., Trends in DNA biosensors. *Talanta* **2008,** *77*, 606-623.
5. Perfézou, M.; Turner, A. P. F.; Merkoçi, A., Cancer detection using nanoparticle-based sensors. *Chem. Soc. Rev.* **2012,** *41*, 2606-2622.
6. Zhu, C. Z.; Yang, G. H.; Li, H.; Du, D.; Lin, Y. H., Electrochemical Sensors and Biosensors Based on Nanomaterials and Nanostructures. *Anal. Chem.* **2015,** *87*, 230-249.
7. Rasheed, P. A.; Sandhyarani, N., Carbon nanostructures as immobilization platform for DNA: A review on current progress in electrochemical DNA sensors. *Biosens. Bioelectron.* **2017,** *97*, 226-237.
8. Hvastkovs, E. G.; Buttry, D. A., Recent advances in electrochemical DNA hybridization sensors. *Analyst* **2010,** *135*, 1817-1829.
9. Lazerges, M.; Bedioui, F., Analysis of the evolution of the detection limits of electrochemical DNA biosensors. *Anal. Bioanal. Chem.* **2013,** *405*, 3705-3714.
10. Qian, Y.; Tang, D. Q.; Du, L. L.; Zhang, Y. Z.; Zhang, L. X.; Gao, F. L., A novel signal-on electrochemical DNA sensor based on target catalyzed hairpin assembly strategy. *Biosens. Bioelectron.* **2015,** *64*, 177-181.
11. Zeng, D. D.; Zhang, H.; Zhu, D.; Li, J.; San, L. L.; Wang, Z. H.; Wang, C. G.; Wang, Y. S.; Wang, L. H.; Zuo, X. L.; Mi, X. Q., A novel ultrasensitive electrochemical DNA sensor based on double tetrahedral nanostructures. *Biosens. Bioelectron.* **2015,** *71*, 434-438.
12. Esteban Fernández de Ávila, B.; Watkins, H. M.; Pingarrón, J. M.; Plaxco, K. W.; Palleschi, G.; Ricci, F., Determinants of the Detection Limit and Specificity of Surface-Based Biosensors. *Anal. Chem.* **2013,** *85*, 6593-6597.
13. Nielsen, P. E.; Egholm, M.; Berg, R. H.; Buchardt, O., Sequence-selective recognition of DNA by strand displacement with a thymine-substituted polyamide. *Science* **1991,** *254*, 1497-1500.
14. Vilaivan, T., Pyrrolidinyl PNA with α/β-Dipeptide Backbone: From Development to Applications. *Acc. Chem. Res.* **2015,** *48*, 1645-1656.
15. Briones, C.; Moreno, M., Applications of peptide nucleic acids (PNAs) and locked nucleic acids (LNAs) in biosensor development. *Anal. Bioanal. Chem.* **2012,** *402*, 3071-3089.
16. Barluenga, S.; Winssinger, N., PNA as a Biosupramolecular Tag for Programmable Assemblies and Reactions. *Acc. Chem. Res.* **2015,** *48*, 1319-1331.
17. Bartold, K.; Pietrzyk-Le, A.; Huynh, T. P.; Iskierko, Z.; Sosnowska, M.; Noworyta, K.; Lisowski, W.; Sannicolo, F.; Cauteruccio, S.; Licandro, E.; D'Souza, F.; Kutner, W., Programmed Transfer of Sequence Information into a Molecularly Imprinted Polymer for Hexakis(2,2'-bithien-5-yl) DNA Analogue Formation toward Single-Nucleotide-Polymorphism Detection. *ACS Appl. Mater. Interfaces* **2017,** *9*, 3948-3958.

18. Hu, Q.; Hu, W. W.; Kong, J. M.; Zhang, X. J., Ultrasensitive electrochemical DNA biosensor by exploiting hematin as efficient biomimetic catalyst toward in situ metallization. *Biosens. Bioelectron.* **2015,** *63*, 269-275.

19. Wang, K.; Sun, Z. L.; Feng, M. J.; Liu, A. L.; Yang, S. Y.; Chen, Y. Z.; Lin, X. H., Design of a sandwich-mode amperometric biosensor for detection of PML/RAR alpha fusion gene using locked nucleic acids on gold electrode. *Biosens. Bioelectron.* **2011,** *26*, 2870-2876.

20. Govindaraju, T.; Kumar, V. A.; Ganesh, K. N., (SR/RS)-Cyclohexanyl PNAs: Conformationally Preorganized PNA Analogues with Unprecedented Preference for Duplex Formation with RNA. *J. Am. Chem. Soc.* **2005,** *127*, 4144-4145.

21. Lucarelli, F.; Marrazza, G.; Turner, A. P.; Mascini, M., Carbon and gold electrodes as electrochemical transducers for DNA hybridisation sensors. *Biosens. Bioelectron.* **2004,** *19*, 515-530.

22. Lucarelli, F.; Tombelli, S.; Minunni, M.; Marrazza, G.; Mascini, M., Electrochemical and piezoelectric DNA biosensors for hybridisation detection. *Anal. Chim. Acta* **2008,** *609*, 139-159.

23. Liu, J.; Tian, S.; Nielsen, P. E.; Knoll, W., In situ hybridization of PNA/DNA studied label-free by electrochemical impedance spectroscopy. *Chem. Commun.* **2005**, 2969-2971.

24. Raoof, J. B.; Ojani, R.; Golabi, S. M.; Hamidi-Asl, E.; Hejazi, M. S., Preparation of an electrochemical PNA biosensor for detection of target DNA sequence and single nucleotide mutation on p53 tumor suppressor gene corresponding oligonucleotide. *Sens. Actuators, B* **2011,** *157*, 195-201.

25. Reisberg, S.; Dang, L. A.; Nguyen, Q. A.; Piro, B.; Noel, V.; Nielsen, P. E.; Le, L. A.; Pham, M. C., Label-free DNA electrochemical sensor based on a PNA-functionalized conductive polymer. *Talanta* **2008,** *76*, 206-210.

26. Thipmanee, O.; Samanman, S.; Sankoh, S.; Numnuam, A.; Limbut, W.; Kanatharana, P.; Vilaivan, T.; Thavarungkul, P., Label-free capacitive DNA sensor using immobilized pyrrolidinyl PNA probe: Effect of the length and terminating head group of the blocking thiols. *Biosens. Bioelectron.* **2012,** *38*, 430-435.

27. Boussicault, F.; Robert, M., Electron Transfer in DNA and in DNA-Related Biological Processes. Electrochemical Insights. *Chem. Rev.* **2008,** *108*, 2622-2645.

28. Sosnowska, M.; Pieta, P.; Sharma, P. S.; Chitta, R.; Kc, C. B.; Bandi, V.; D'Souza, F.; Kutner, W., Piezomicrogravimetric and Impedimetric Oligonucleotide Biosensors Using Conducting Polymers of Biotinylated Bis(2,2′-bithien-5-yl)methane as Recognition Units. *Anal. Chem.* **2013,** *85*, 7454-7461.

29. Voccia, D.; Sosnowska, M.; Bettazzi, F.; Palchetti, I.; Kutner, W., Label-Free Impedimetric Determination of miRNA Using Biotinylated Conducting Polymer Modified Carbon Electrodes. In *Sensors*, Compagnone, D.; Baldini, F.; DiNatale, C.; Betta, G.; Siciliano, P., Eds. Springer: New York, 2015; Vol. 319, pp 59-64.

30. Gestwicki, J. E.; Hsieh, H. V.; Pitner, J. B., Using Receptor Conformational Change To Detect Low Molecular Weight Analytes by Surface Plasmon Resonance. *Anal. Chem.* **2001,** *73*, 5732-5737.

Table 1. Thermodynamic parameters determined from ITC of GCGGCGGC PNA **1** titration with cytosine **2** or guanine **3** functional monomer. The binding parameters of PNA-(functional monomer) interactions were determined by ITC data fitting with a theoretical isotherm of ([a]) the multiple and ([b]) independent binding sites model.

Complex stability constant, K_s M^{-1}	ΔH kJ mol^{-1}	ΔG kJ mol^{-1}	ΔS J mol^{-1} K^{-1}	Number of nucleobase binding sites of PNA bound to functional monomer
$K_{s,1}$ (GCGGCGGC-**2**)[a] = 10^7	-102.0	-40.6	-206.0	1st step: three guanine moieties
$K_{s,2}$ (GCGGCGGC-**2**)[a] = 9.0×10^5	-34.3	-34.0	-1.0	2nd step: next two guanine moieties
K_s (GCGGCGGC-**3**)[b] = 1.5×10^5	-3.7	-29.5	86.7	Three cytosine moieties

[a] 75 μM **1** was titrated with 4.0 mM **2** in DMSO.
[b] 30 μM **1** was titrated with 0.70 mM **3** in DMSO.

Table 2. The EIS determined matrix effect for the GCGGCGGC DNA in Dulbecco Modified Eagle Medium (DMEM).

Sample No.	$c_{GCGGCGGC}$ in DMEM, determined, nM	$c_{GCGGCGGC}$ in PBS (pH = 7.4), determined, nM	Matrix effect, %
1.	2.68	2.99	89.63
2.	7.56	7.93	95.33
3.	38.82	33.81	114.81
4.	54.61	52.13	104.76
5.	71.10	69.77	101.90
Average			101.29

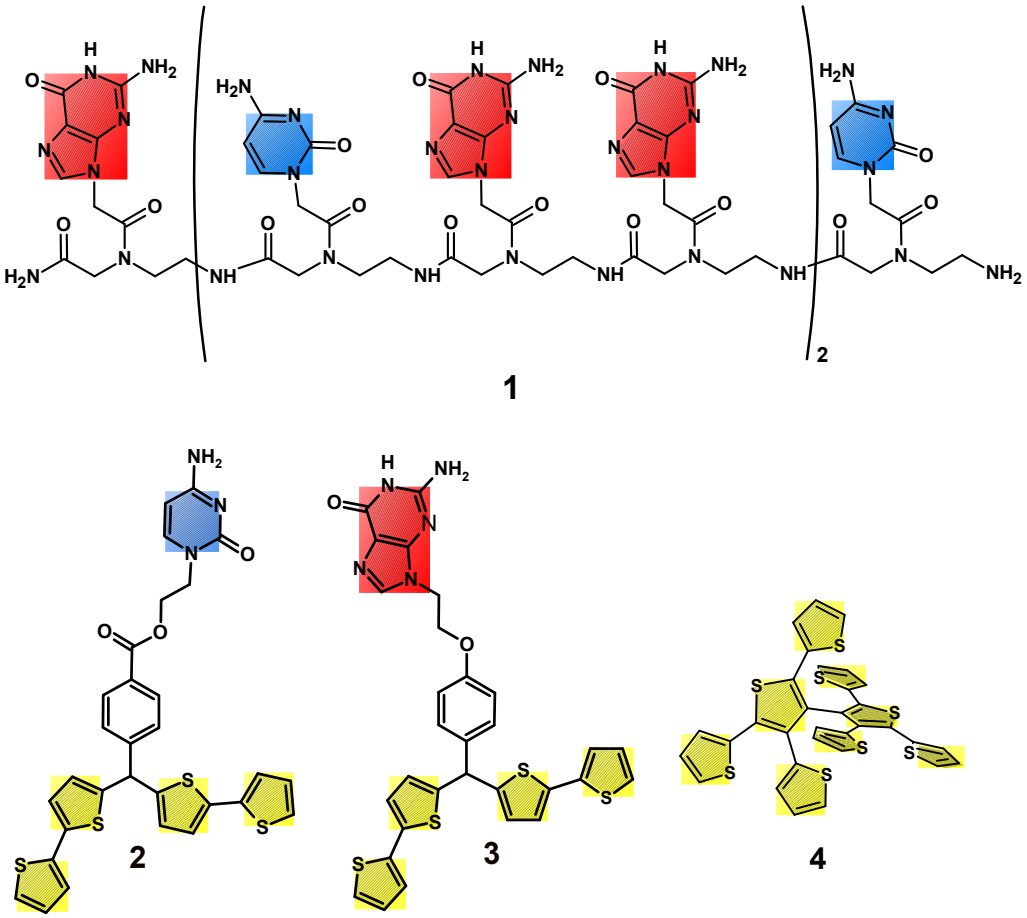

Scheme 1. Structural formulas of *C*-term-GCGGCGGC-*N*-term single-stranded PNA **1**, 2-(cytosin-1-yl)ethyl 4-*bis*(2,2'-bithien-5-yl)methylbenzoate **2** and 4-*bis*(2,2'-bithien-5-yl)methylphenyl-2-guanine ethyl ether **3** functional monomers as well as the 2,4,5,2',4',5'-*hexa*(thiophene-2-yl)-3,3'-bithiophene **4** cross-linking monomer.

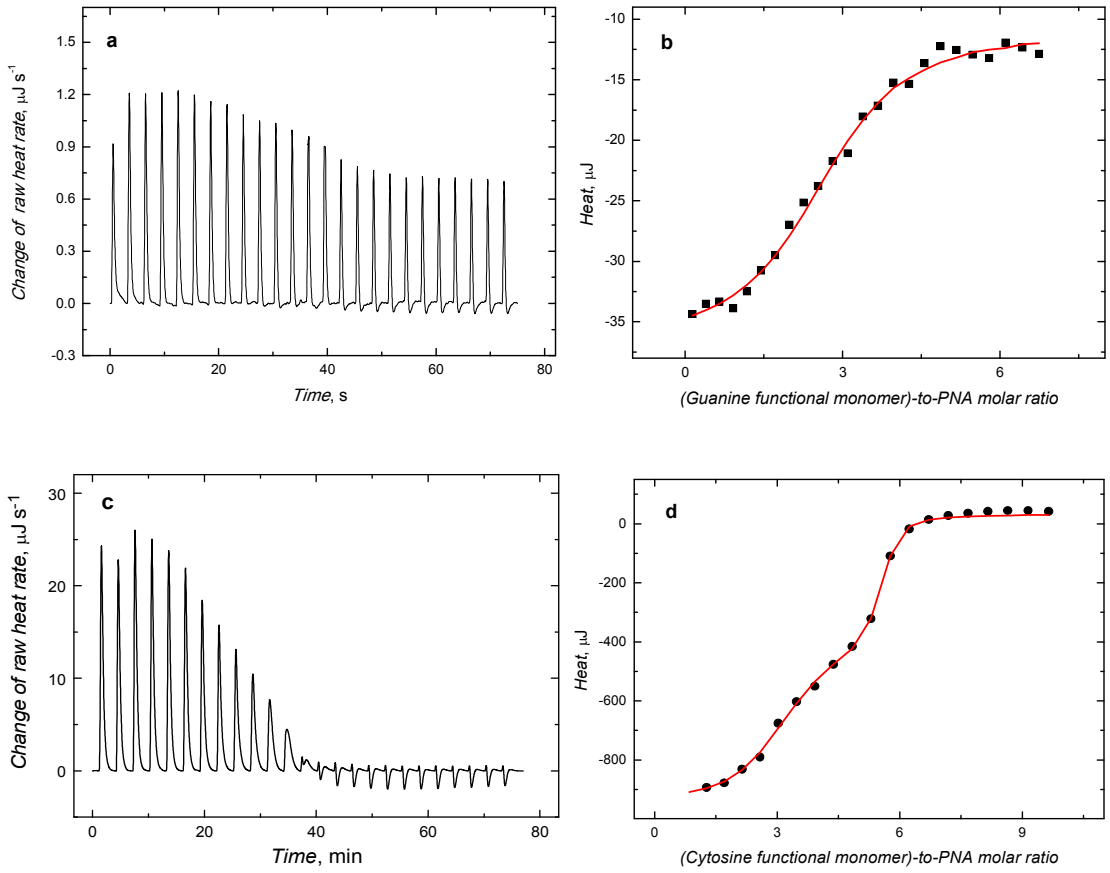

Figure 1. The ITC raw heat rate change with time after consecutive addition of 8-μL aliquots of (a) 0.70 mM guanine functional monomer **3** and (c) 4.0 mM cytosine functional monomer **2** in DMSO to (a) 30 μM and (c) 75 μM PNA **1** in DMSO at 3-min intervals. The binding isotherms for these titrations are represented by curves of the least-square fit of (b) an independent and (d) a multiple binding sites model to the data acquired.

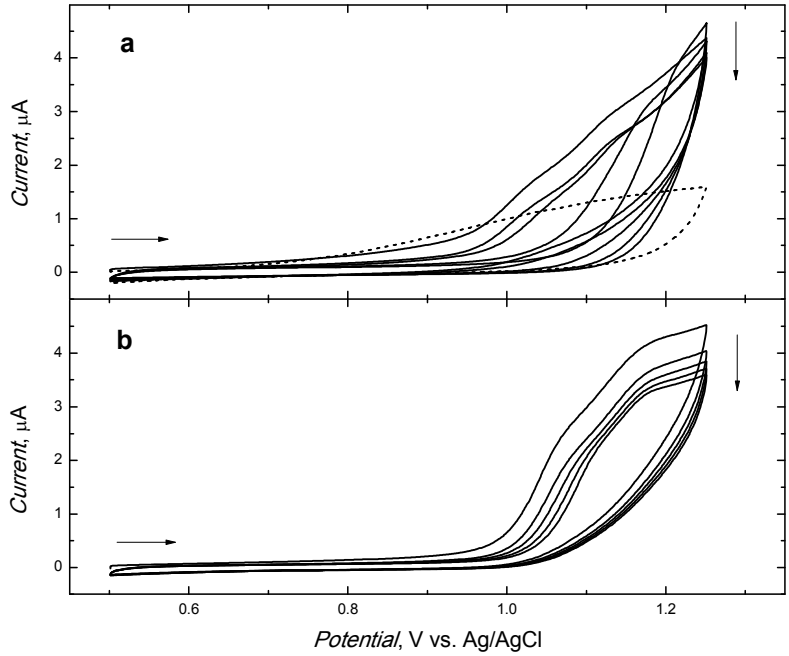

Figure 2. (a, dash curve) The potentiodynamic curve for 0.05 mM PNA **1** and 0.1 M (TBA)ClO_4 in the acetonitrile-water, 9:1 (*v*/*v*), solution recorded at the 1-mm diameter Pt disk electrode. (a, solid curves) The multi-cycle potentiodynamic curve for simultaneous electropolymerization and deposition on the Pt disk electrode of the PNA-templated MIP film from the 0.02 mM **1**, 0.1 mM **2**, 0.06 mM **3**, and 0.1 mM **4** in 0.1 M (TBA)ClO_4 acetonitrile-water, 9:1 (*v*/*v*) solution. The potential scan rate was 50 mV s^{-1}. (b) Multi-cyclic potentiodynamic curve for simultaneous electropolymerization and deposition of the NIP film from 0.1 mM **2**, 0.06 mM **3** and 0.1 mM **4** in the 0.1 M (TBA)ClO_4 acetonitrile-water, 9:1 (*v*/*v*), solution.

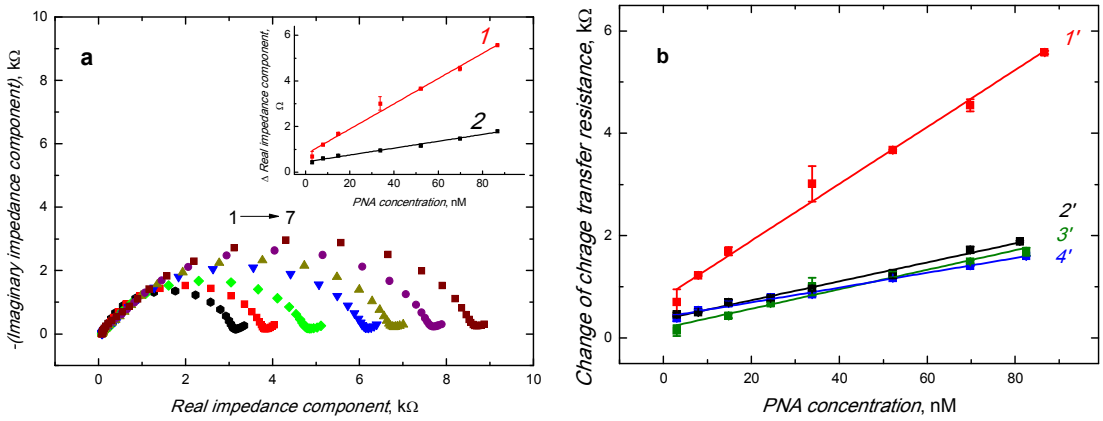

Figure 3. (a) Nyquist plots of impedance spectra for the 1-mm Pt disk electrode coated with the MIP film immersed for 5 min in solutions of the GCGGCGGC DNA analyte of different concentrations. Measurements were performed for the 0.1 M mM PBS (pH=7.4), 0.1 M $[Fe(CN)_6]^{4-}$ and 0.1 M $[Fe(CN)_6]^{3-}$ at the applied potential equal to the open circuit potential. The inset shows calibration plots for the GCGGCGGC DNA analyte at (1) the PNA-extracted MIP and (2) NIP film. (b) Calibration plots constructed using the data obtained by fitting electric parameters of the equivalent circuit to experimental data, for (*1'*) the GCGGCGGC DNA analyte, (*2'*) two-nucleobase mismatched GCG**AT**GGC DNA oligonucleotide, (*3'*) two-nucleobase mismatched GC**T**GC**T**GC PNA oligonucleotide, and (*4'*) three-nucleobase mismatched GCG**ATC**GC PNA.

TOC Graphic

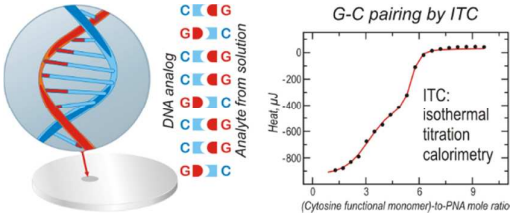
DNA analog
Analyte from solution
G-C pairing by ITC
Heat, μJ
0
-200
-400
-600
-800
0
3
6
9
(Cytosine functional monomer)-to-PNA mole ratio
ITC:
isothermal
titration
calorimetry